electronics

MDPI

Article

Neutron Irradiation Testing and Monte Carlo Simulation of a Xilinx Zynq-7000 System on Chip

Weitao Yang [1,2,3], Yonghong Li [2,*], Yang Li [2], Zhiliang Hu [2,4,5], Jiale Cai [6], Chaohui He [2], Bin Wang [1,*] and Longsheng Wu [1]

1 School of Microeletronics, Xidian University, Xi'an 710071, China
2 School of Nuclear Science & Technology, Xi'an Jiaotong University, Xi'an 710049, China
3 Dipartimento di Automatica e Informatica, Politecnico di Torino, 10129 Torino, Italy
4 Spallation Neutron Source Science Center, Dongguan 523803, China
5 Institute of High Energy Physics, Chinese Academy of Sciences (CAS), Beijing 100049, China
6 Dipartimento di Elettronica e Telecomunicazioni, Politecnico di Torino, 10129 Torino, Italy
* Correspondence: yonghongli@mail.xjtu.edu.cn (Y.L.); wbin@xidian.edu.cn (B.W.)

Abstract: The reliability of nanoscale electronic systems is important in various applications. However, they are becoming increasingly vulnerable to atmospheric neutrons. This research conducted spallation neutron irradiations on a Xilinx Zynq-7000 system on a chip using the China Spallation Neutron Source. The results were analyzed in combination with a Monte Carlo simulation to explore the impact of atmospheric neutrons on the single event effects of the target system on chip. Meanwhile, the contribution of thermal neutrons to the chip's single event effect susceptibility was also assessed. It was found that absorbing thermal neutrons with a 2 mm Cd sheet can protect against the single event effect on the system on the chip by about 44.4%. The effects of B and Hf elements, inside the device, on a single event effect of the Xilinx Zynq-7000 system on chip were evaluated too. Additionally, it was discovered that ^{10}B interacting with thermal neutrons was the primary cause of the thermal neutron-induced single event effect in the system on chip. Although Hf has a high neutron capture cross section, its presence does not significantly affect the sensitivity to single event effects. However, during atmospheric neutron irradiation, the presence of Hf increases the possibility of depositing the total dose in the tested chip.

Keywords: spallation neutron; thermal neutron; Monte Carlo; system on chip; single event effect

Citation: Yang, W.; Li, Y.; Li, Y.; Hu, Z.; Cai, J.; He, C.; Wang, B.; Wu, L. Neutron Irradiation Testing and Monte Carlo Simulation of a Xilinx Zynq-7000 System on Chip. *Electronics* **2023**, *12*, 2057. https://doi.org/10.3390/electronics12092057

Academic Editor: Paul Leroux

Received: 3 April 2023
Revised: 23 April 2023
Accepted: 26 April 2023
Published: 29 April 2023

1. Introduction

The atmospheric neutron comes from the interaction of cosmic rays with the atmospheric nuclei. These neutrons have a wide range of energies, ranging from thermal neutron to GeV [1]. In the past decades, this has been serious concern in the field of avionics, regarding atmospheric neutrons resulting in single event effects (SEE) [2,3]. As semiconductor manufacturing technology rapidly develops, concerns have also shifted to the potential of atmospheric neutrons to cause single event effects (SEE) in terrestrial electronic systems [4–6].

The sensitivity of electronic systems to atmospheric neutrons can be explored in two ways [7]. One involves conducting high altitude tests in real atmospheric environments. For instance, Xilinx's Rosetta experiment assessed the soft errors of various technology field programmable gate arrays in different locations globally in the past few years [8–10]. Similarly, in China, Chen et al. investigated the real-time atmospheric neutron induced soft errors on different static random access memories at the Yangbajing international cosmic ray observatory of the Chinese Academy of Science in Tibet, China [11–13]. However, the major drawback of this method is that it can be quite time consuming, even though the results obtained are the most authentic.

The other method involves performing irradiation tests using various irradiation equipment to evaluate the effects of years of exposure in real surroundings in just a few hours with intense flux [7]. This can be achieved by using sources such as a reactor, monoenergetic neutrons, and spallation neutrons [14]. Among these, spallation neutrons are considered to be closer to the real situation and are the ideal surrogate for accelerating atmospheric neutron SEE tests when compared to the former two [15]. In addition, by spallation neutron irradiation, it is possible to conduct a more comprehensive analysis on the total single-event effects (SEE) caused by atmospheric neutrons, including the assessment of the contribution of different energy ranges of neutrons [16]. For instance, the assessment of SEE soft errors comes from the thermal neutron, the neutron above 1 or 10 MeV. In particular, it is more convenient to further investigate the impact of thermal neutrons on an atmospheric environment.

In 2001, R. C. Baumann was the first to report that ^{10}B interacting with the thermal neutron is a dominant factor in soft errors for deep-submicron static random access memory with borophosphosilicate glass (BPSG) packages [17]. Since then, advanced integrated circuit development has led to chip packages no longer requiring the BPSG package [18–20]. However, for the nanoscale electronic systems, even though the BPSG package is no longer used, they still face the threats of ^{10}B interacting with thermal neutrons [21–24]. This is because ^{10}B contamination might occur in the semiconductor contact and doping processes, and the rapidly developed semiconductor manufacturing technology pushes the supply voltage and SEE critical charges lower and lower.

In [21], M. Cecchetto et al. pointed out that the thermal neutron can induce almost 90% of upset events in some cases. In [22], C. Weulersse et al. analyzed the SEE soft errors for 90, 65, and 28 nm technology memories under thermal and high energy neutron conditions, and confirmed that 28 nm technology devices are strongly impacted by the thermal neutron. Recent research has investigated the influence of ^{10}B contamination on SEE susceptibility by exposing a 65 nm technology microcontroller unit to thermal and high-energy neutrons at the China Spallation Neutron Source [25]. The results showed that ^{10}B interacting with thermal neutrons dominated the atmospheric neutron SEE in the device, with a SEE ratio of 1.89:1 induced by thermal and higher energy neutrons on the 65 nm technology microcontroller unit [25].

The 65 nm technology microcontroller unit test results in our previous work also indicate that the interaction of ^{10}B with thermal neutrons is still a serious concern for advanced integrated chips. Additionally, the obtained results have also further motivated us to explore the thermal neutron impact on the smaller technology system on chip using China spallation neutron source, for instance, the Xilinx Zynq-7000 system on chip (SoC) which is manufactured with the 28 nm complementary metal oxide semiconductor (CMOS) technology.

For the Xilinx Zynq-7000 SoC thermal neutron SEE analysis, in addition to the possible boron contamination, another element should also be considered. This element is the hafnium (Hf) element. Compared to boron (B), the neutron capture cross section with Hf is higher at several eV intervals. Figure 1 displays the neutron cross section spectra of ^{10}B (19.9% abundance), ^{178}Hf (27.1% abundance), and ^{28}Si (92.2% abundance) [26]. It can be seen that the peak cross section of ^{178}Hf even reaches 10^5 barns. The cross sections of ^{178}Hf with thermal neutrons are also higher than those of ^{28}Si by two orders of magnitude. Another significant fact is that the element boron exists in the Xilinx Zynq-7000 SoC as a result of contamination from manufacturing processes; however, its region cannot be confirmed by measurements such as secondary ion mass spectrometry. Hafnium is different from the element boron, and does indeed exist in the high-K dielectric materials used in the manufacturing of the Xilinx Zynq-7000 SoC. This makes the atmospheric neutron-induced SEE assessment on the Xilinx Zynq-7000 SoC even more complicated.

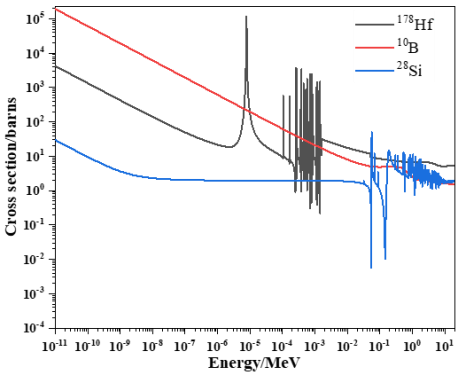

Figure 1. The cross sections of the neutron with ^{10}B (19.9% abundance), ^{178}Hf (27.1% abundance), and ^{28}Si (92.2% abundance) [26].

The atmospheric neutron-induced SEE on the Xilinx Zynq-7000 SoC was examined via an irradiation test conducted at the China Spallation Neutron Source (CSNS)-BL09 [27]. In the irradiation test, the Xilinx Zynq-7000 SoC chip was directly exposed to the ejected neutron beam without any shielding, which covered both thermal and high-energy components. To achieve a deeper understanding of the atmospheric neutron SEE on the Xilinx Zynq-7000 SoC, a second irradiation was conducted with the inclusion of a 2 mm cadmium (Cd) sheet to absorb the thermal neutrons in front of the chip. By comparing the results of the two irradiation tests, it is possible to investigate the contribution of thermal neutrons to the tested SoC. Furthermore, the impact of elements such as B and Hf can be analyzed through both irradiation and Monte Carlo simulations.

2. Irradiation Tests

As mentioned above, performing an actual atmospheric neutron SEE test would be time consuming, and the spallation neutron source is the closest to the real atmospheric neutron spectrum. The implementation of the China Spallation Neutron Source in 2018 has made it convenient to conduct atmospheric neutron SEE tests in China using the spallation neutron source [28]. We have obtained some SEE test results from [25,27]. Figure 2 illustrates the calculated differential flux of the neutron beam from the China Spallation Neutron Source (CSNS) (10^9 for the Beijing terrestrial system). The CSNS spectrum is very similar to that of the atmospheric neutron spectrum at sea level, as observed for the Beijing terrestrial system, though larger by a factor of 10^9. In the actual environment, even though the neutron spectrum impinging on a chip will be different from the spallation neutron beam due to the surrounding factors, the detected results are close to the actual situation.

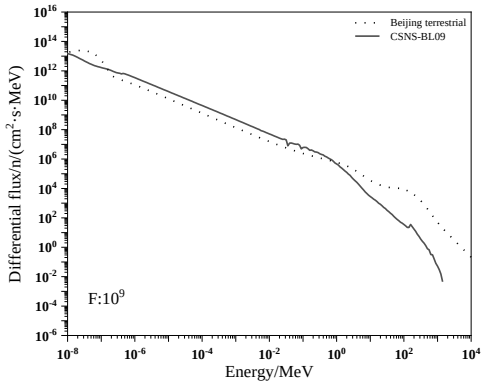

Figure 2. The differential flux of the neutron beam at CSNS [25,27,29].

Two separate irradiation tests were performed on the same series Xilinx Zynq-7000 SoC using the CSNS-BL09 facility. In the first test (described in reference [27]), the tested SoC was exposed to the neutron beam without any shielding. In the second test, which

is the main effort of this work, a 2 mm thick Cd sheet was inserted between the beam ejection stop and the tested chip to absorb thermal neutrons. The effectiveness of the sheet in absorbing neutrons with energies below 0.5 eV is demonstrated in Figure 3, which shows a comparison of the neutron spectrum at the terminal with and without the Cd sheet. In Figure 3, the spectrum of CSNS-BL09 + 2 mm Cd is measured behind the 2 mm Cd sheet before the irradiation test. Even though the thermal neutron that interacts with the Cd might produce some new neutrons, the figure indicates that the neutron fluence was reduced by two to three orders of magnitude with the 2 mm Cd sheet shielding in place at energies lower than 0.5 eV.

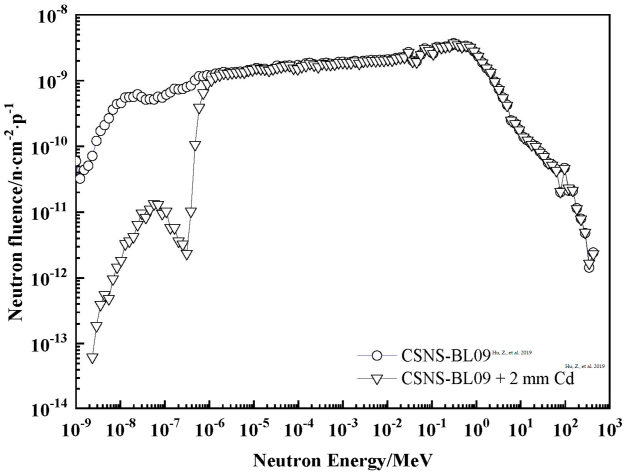

Figure 3. Neutron fluence with and without 2 mm Cd sheet [25].

The on-chip memory (OCM) block of the Xilinx Zynq-7000 SoC (Xilinx-Zynq 7020 CLG484) was examined in the first irradiation. For comparison, it was tested in this work again. The 64 kB data stored in the OCM were dynamically tested; the checked pattern data were written into the OCM addresses and subsequently read back by the SoC. The read back data were compared with the check pattern data to identify any SEE. The comparison results were transferred to a PC and displayed in a terminal. To allow for comparison with the first irradiation, which examined the normal condition without any SEE mitigation techniques, the same conditions were replicated in this effort.

The test setups for both irradiation tests were almost identical, except for the addition of a 2 mm Cd sheet in the second test to absorb thermal neutrons. The test board was powered by a 2260B programming DC power supply, and the real-time current was monitored and recorded by a remote host computer. Additionally, potential single event latch-up was monitored during the tests. Communication between the host computer and test board was established through a universal serial bus cable, and running messages were recorded in real-time.

3. Results and Discussions

During both irradiations, four types of soft errors were detected: single bit upset (SBU), dual cell upset (DCU), multi-cell upset (MCU), and single event functional interruption (SEFI). No abnormal current was detected, indicating that no latch-up event occurred during the atmospheric neutron SEE irradiation tests of the chip. However, there were discrepancies between the two irradiations in terms of SEE cross section, suggesting that thermal neutrons had an impact on the Xilinx Zynq-7000 SoC during the atmospheric neutron irradiation tests.

3.1. Detected Events

In the current irradiation test, 19 events were detected. Table 1 presents the number of each type of error, with SBU events being the most frequent, which is similar to the

first irradiation. During the current irradiation, the neutron flux above 1 MeV was approximately 6.85 $\times$ 10^5 n·cm^{-2}·s^{-1}, and the corresponding fluence was 2.47 $\times$ 10^{10} n·cm^{-2}. As a result, the SBU cross section was calculated to be (5.26 $\pm$ 0.26) $\times$ 10^{-10} cm^2 and (1.00 $\pm$ 0.05) $\times$ 10^{-15} cm^2·bit^{-1} for the irradiation with few thermal neutrons.

Table 1. The detected SEE in irradiation with few thermal neutrons.

SBU	DCU	MCU	SEFI
13	2	2	2

Figure 4 displays the detected SEE during the first irradiation [27]. The figure shows the number of SBU 21, which is the highest among all types of events. Table 1 and Figure 4 show that SBU events dominate the detected soft errors in both irradiations.

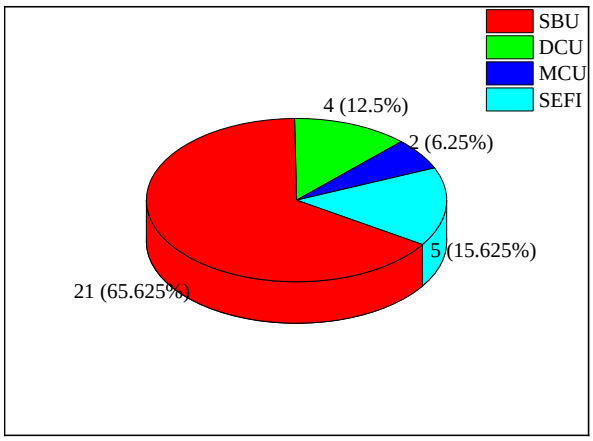

Figure 4. The detected numbers of different SEE in the first irradiation test at CSNS-BL09 [27].

Table 2 presents the SBU cross sections for two different irradiations.

Table 2. The SBU cross sections in two irradiations [27].

Neutron Beam	Fluence 10^{10} cm^{-2}	SBU	Cross Section 10^{-10} cm^2	Bit Cross Section 10^{-15} cm^2·bit^{-1}
CSNS-BL09 [27]	2.22	21	9.46 $\pm$ 0.47	1.80 $\pm$ 0.09
CSNS-BL09 + 2 mm Cd	2.47	13	5.26 $\pm$ 0.26	1.00 $\pm$ 0.05

In the current irradiation, the neutron fluence is 2.47 $\times$ 10^{10} n·cm^{-2}, which is 11.26% higher than in the first irradiation. Surprisingly, the number of SBU events is only 13 in the current irradiation, whereas it was more in the first irradiation, achieving 21. In general, a high fluence should correspond to a high number of SEE, this anomaly indicates that thermal neutrons may be contributing to the atmospheric neutron SEE on the tested SoC. The difference in bit cross sections between the two irradiations is 0.8 $\times$ 10^{-15} cm^2·bit^{-1}, which could be attributed to the shielding of thermal neutrons in the second irradiation. According to Formula (1), this indicates that shielding thermal neutrons with a 2 mm Cd sheet could make the SEE cross section smaller by about 44.4%. These findings demonstrate that the impact of thermal neutrons cannot be disregarded when it comes to SEE caused by atmospheric neutrons in the Xilinx Zynq-7000 SoC, even though the tested chips no longer employ BPSG in their packaging.

$$d = \frac{\sigma - \xi}{\sigma} \quad (1)$$

where d is the discrepancy, σ and ξ are the bit cross section of the first and the current irradiation test with cm^2·bit^{-1}.

3.2. B Influence

The atmospheric neutron irradiation test results of the 65 nm technology microcontroller unit showed that secondary particles from thermal neutrons interacting with ^{10}B could cause SEU in advanced electronic systems and make a significant contribution to the SEE cross section. When compared to the 65 nm technology memory cell, the SEU critical charge of the 28 nm complementary metal oxide semiconductor technology memory cells is lower, making the Xilinx Zynq-7000 SoC memory cells more susceptible to soft errors induced by thermal neutrons.

$$^{10}B + n_{th} \rightarrow ^{7}Li(1.01\ MeV) + \alpha(1.78\ MeV) \quad (2)$$

$$^{10}B + n_{th} \rightarrow ^{7}Li(0.84\ MeV) + \alpha(1.47\ MeV) + \gamma(0.48\ MeV) \quad (3)$$

The sum of the energies of generated secondary α and ^{7}Li is constant. They are located within a determined region in the pulse amplitude distribution spectrum. Formulas (2) and (3) describe the mechanisms of the thermal neutron (nth) interacting with ^{10}B. The probability of (2) is 6%, while that of (3) is 94% [30,31]. In (3), although 0.48 MeV γ is also produced, unlike the generated ^{7}Li and α ions, it is uncharged. It needs to generate secondary electrons or other ionization particles to trigger SEE; this case's probability is rather low. In addition, the γ ray has a high penetration depth, making it deposit energy over a long trajectory, while the size of the sensitive volume of 28nm technology memory cells is extremely small. This means the sensitive volume cannot collect as many charges to induce SEE when a gamma ray passes. Thus, SEE induced by the produced gamma ray can be disregarded here. Given the above analysis, it could be speculated that the key factors of SEE cross section discrepancy on the tested SoC are generated by the secondary α and ^{7}Li. Table 3 illustrates the ranges and linear energy transfers (LETs) of the generated ionized secondary particles in silicon [32].

Table 3. The ranges and LETs of secondary particles of ^{10}B with the thermal neutron.

Range in Silicon/μm				**LET/MeV·cm^2·mg^{-1}**			
^{7}Li		**α**		**^{7}Li**		**α**	
0.84 MeV	1.01 MeV	1.47 MeV	1.78 MeV	0.84 MeV	1.01 MeV	1.47 MeV	1.78 MeV
2.50	2.80	5	6.36	2.10	2.16	1.15	1.06

Due to the significant discrepancy between Formulas (3) and (2), the following analysis will primarily focus on the secondary particles of (3), which are similar to (2). The α (1.47 MeV) and ^{7}Li (0.84 MeV) ions have ranges of only 5 μm and 2.5 μm in silicon, respectively. These are much lower than the thickness of the Xilinx Zynq-7000 SoC from its top passive layers to the substrate's surface [33]. This phenomenon suggests that ^{10}B contamination indeed exists within the chip, which is approaching the sensitive volumes of the memory cell of the SoC. The SEE LET threshold of the 28 nm CMOS memory cell is approximately 0.50 MeV·cm^2·mg^{-1} [34]. This is because the LETs are about 2.10 and 1.15 MeV·cm^2·mg^{-1} for the ^{7}Li (0.84 MeV) and α (1.47 MeV), respectively, meaning they are higher than the threshold. This means that both secondary particles can induce SEE in the tested SoC.

The current tested Xilinx Zynq-7000 SoC also includes the Hf element in the high-K dielectric materials. Furthermore, the cross section of the Hf element with the thermal neutron is greater than that of silicon. As a result, it is not yet possible to conclude that the disparity between the two can be attributed solely to the presence or absence of ^{10}B.

3.3. Hf Influence

^{10}B interacts with thermal neutrons, leading to SEE primarily caused by nuclear reactions. Meanwhile, the main interaction between the thermal neutron and the Hf

element is the (n, γ) reaction, as depicted in Figure 5, which produces γ-rays that typically result in the total ionizing dose rather than SEE in the device [35]. As mentioned above, the possibility of SEE occurring from the interaction between generated γ-rays is relatively low.

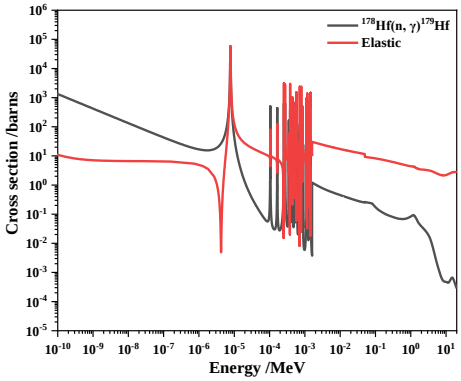

Figure 5. Neutron cross section spectrums of (n, γ) and elastic reactions with ^{178}Hf [26].

The cross sections of ^{178}Hf interacting with eV-level neutrons are remarkably high, reaching 10^5 barns when compared to high-energy neutrons. Therefore, it is crucial to thoroughly evaluate whether the presence of hafnium in the tested SoC contributes to atmospheric neutron-induced SEE.

While the contribution of the (n, γ) reaction to the induction of SEE in the SoC is relatively low, there is a potential for the transfer of energy from neutrons to hafnium nuclei in elastic interactions, which may increase the likelihood of causing SEE. The maximum transfer energy to the Hf nuclei from a neutron can be calculated using Formula (4) [36].

$$\mathrm{Et} = \frac{4\mathrm{MnMt}}{(\mathrm{Mn} + \mathrm{Mt})^2}\mathrm{En} \tag{4}$$

Et is the max energy transfer to Hf nuclei with keV; Mn is the mass of the neutron, which is 1.67×10^{-27} kg; Mt is the Mass of Hf and it is 2.96×10^{-25} kg; and En is the energy of neutron with keV.

The focus of this article is on SEE soft errors for the Xilinx Zynq-7000 SoC induced by thermal neutrons reacting with boron and hafnium elements. As stated in Section 2, neutrons with an energy lower than 0.5 eV are absorbed by the inserted 2 mm Cd sheet. For the 0.5 eV neutron, the maximum energy transferred to the Hf atom is approximately 0.01 eV. The resonance in the Hf cross section has a high peak, while being intensely narrow. Additionally, even with an extension of the neutron energy to the rightmost peak, the corresponding maximum energy transferred is lower than 0.03 keV. Based on their corresponding LET values (which are lower than 0.50 MeV·cm^2·mg^{-1}), it is unlikely that they would result in SEE on the tested SoC. Therefore, the high cross section elastic interaction between Hf and thermal and eV neutrons does not have an impact on atmospheric neutron-induced SEE in the Xilinx Zynq-7000 SoC. It can be concluded that the difference in SEE cross section between the two irradiations is mainly caused by the presence of ^{10}B contamination, which indeed exists within the chip. It verifies the thermal neutron's influence on the nanoscale device's SEE susceptibility again.

3.4. Monte Carlo Simulation

The thickness and materials of the passive layers on the cut cross section of the chip were obtained [27,33]. The 28 nm high-K metal gate technology consists of TiN (8 nm), HfO_2 (10 nm), and SiON (1.2 nm) [37]. Additionally, the ultra-thin SiON layer in the high-k metal gate technology can also be an ultra-thin SiO_2 layer [38]. Based on this information, two Geant4 Monte Carlo simulation models were developed to examine the influence of the Hf element [39,40]. In Figure 6a, only the TiN and ultra-thin SiO_2 layers were considered in the first model, while in Figure 6b, the TiN, HfO_2, and ultra-thin SiO_2 layers were

considered simultaneously in the second model. The remaining parameters for the two simulation models are the same. As trace amounts of boron impurities may be introduced by manufacturing processes or other means, and their abundance and region cannot be determined precisely, boron was not considered in the simulation.

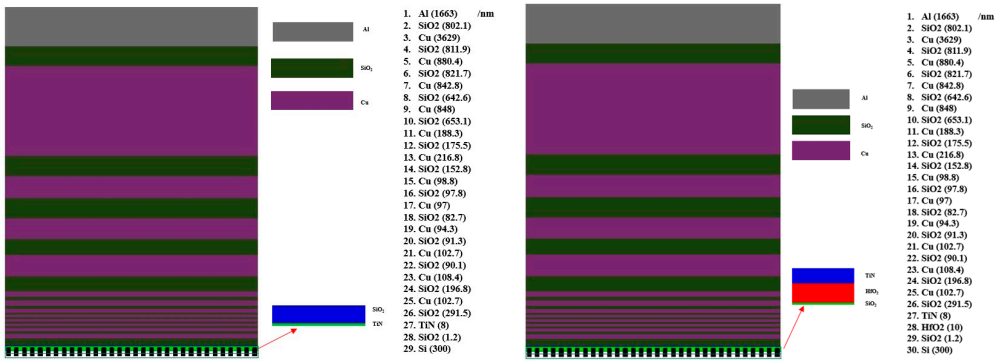

(**a**) (**b**)

Figure 6. The two built Geant4 simulation models. (**a**) TiN and ultra-thin SiO_2 layers above the substrate, (**b**) TiN, HfO_2, and ultra-thin SiO_2 layers above the substrate.

In the simulation, the spectrum of neutron sources accurately reflects that of the first irradiation test, comprising both thermal and high energy neutrons. The model's surface area measures 10 µm × 10 µm, and contains a total of 10^7 neutrons. To detect single event upsets (SEUs), 32 × 32 sensitive volumes (SVs) have been strategically placed throughout the geometry, with each SV measuring 130 nm × 130 nm × 130 nm. An SEU is detected when the deposited energy in an SV exceeds the critical charge of 0.18 fC.

Table 4 presents the recorded number of the detected SEU events in the cells and the deposited doses in the ultra-thin SiO_2 layer in both simulations. The results show that the number of upset events and the cross section remain consistent between the two simulations. However, the deposited total dose in the ultra-thin SiO_2 layers differs by almost five times. This confirms that the presence of the Hf element does not impact the Xilinx Zynq-7000 SoC atmospheric neutron's SEE vulnerability. Nevertheless, the existence of hafnium may increase the total deposited dose during atmospheric neutron SEE irradiation, as highlighted by the high (n, γ) cross section shown in Figure 5. The larger number of γ rays implies a greater potential for total ionization dose on the examined SoC. These simulation results support the need for total dose threat monitoring in future high fluence atmospheric neutron SEE irradiation tests for similar series SoC.

Table 4. The upset number and deposited doses in two simulations.

Upset Number		Bit Cross Section/cm^2·bit^{-1}		Deposited Dose/rad	
First Model	Second Model	First Model	Second Model	First Model	Second Model
5	5	5×10^{-16}	5×10^{-16}	12.6	63.3

Based on the first model, the gamma ray striking simulation has also been executed, but no SEE events were detected. This confirms that the SEE cross section discrepancy between the two irradiations is produced by B interacting with thermal neutron.

The current two built models aimed to examine the influence of Hf on the SEE sensitivity of the Xilinx Zynq-7000, and this was achieved (five times total dose discrepancy was observed). In the future, if the information about the boron contamination could also be further confirmed in the SoC, the update models could be constructed and more detailed simulations could be executed. In addition, if possible, different energies of gamma ray striking experiments could be performed to investigate gamma influence on the SEE and confirm the findings of the current effort further.

4. Conclusions

The Xilinx Zynq-7000 SoC manufactured with 28 nm CMOS technology was exposed to two rounds of spallation neutron irradiation at CSNS-BL09. In the first irradiation, the spectrum covered both thermal and high-energy neutron components, while the second irradiation shielded thermal neutrons. The analysis of both irradiation tests revealed discrepancies. These discrepancies should be attributed to the interaction of ^{10}B with thermal neutrons. To mitigate the sensitivity of the Xilinx Zynq-7000 SoC to atmospheric neutron single event effects, a 2 mm Cd sheet can be employed to shield thermal neutrons against SEE sensitivity by approximately 44.4%. Although hafnium indeed exists in the Xilinx Zynq-7000 SoC and has a high interaction cross section with thermal neutrons, it does not affect atmospheric neutron SEE. However, it is important to pay attention to the total dose hazard during simulated atmospheric neutron SEE irradiation, as hafnium can increase the probability of a deposited total dose.

Author Contributions: Conceptualization, W.Y. and C.H.; methodology, Y.L.(Yonghong Li); software, Y.L.(Yang Li), J.C.; validation, Z.H.; formal analysis, L.W.; resources, Z.H.; writing—original draft preparation, W.Y and B.W. All authors have read and agreed to the published version of the manuscript.

Funding: This project was supported by the National Natural Science Foundation of China (Grant Nos. 11835006, 11690040, and 11690043), Natural Science Basic Research Plan in the Shaanxi Province of China (Grant No. 2023-JC-QN-0015), and the Fundamental Research Funds for the Central Universities (Grant No. XJSJ23049).

Data Availability Statement: The data used to support the findings of this study are available from the corresponding author upon request.

Conflicts of Interest: The authors declare no conflict of interest.

References

1. Dyer, C.; Hands, A.; Ford, K.; Frydland, A.; Truscott, P. Neutron-induced single event effect testing across a wide range of energies and facilities and implications for standards. *IEEE Trans. Nucl. Sci.* **2006**, *53*, 3596–3601. [CrossRef]
2. Normand, E. Single-Event Effects in Avionics. *IEEE Trans. Nucl. Sci.* **1996**, *43*, 461–474. [CrossRef]
3. Leray, J.L. Effects of atmospheric neutrons on devices, at sea level and in avionics embedded systems. *Microelectron. Reliab.* **2007**, *47*, 1827–1835. [CrossRef]
4. Song, Y.; Tu, X.; Li, Z. A Detection Method of Atmospheric Neutron Profile for Single Event Effects Analysis of Civil Aircraft Design. *Atmosphere* **2022**, *13*, 1441. [CrossRef]
5. Baumann, R.C. Landmarks in Terrestrial Single-Event Effects. In Proceedings of the Nuclear and Space Radiation Effects Conference (NSREC), San Francisco, CA, USA, 8–12 July 2013.
6. Autran, J.L.; Munteanu, D.; Roche, P.; Gasiot, G.; Martinie, S.; Uznanski, S.; Sauze, S.; Semikh, S.; Yakushev, E.; Rozov, S.; et al. Soft-errors induced by terrestrial neutrons and natural alpha-particle emitters in advanced memory circuits at ground level. *Microelectron. Reliab.* **2010**, *50*, 1822–1831. [CrossRef]
7. Bisello, D.; Candelori, A.; Dzysiuk, N.; Mastinu, P.; Mattiazzo, S.; Prete, G.; Silvestrin, L.; Wyss, J. Neutron production targets for a new Single Event Effects facility at the 70 MeV Cyclotron of LNL-INFN. *Phys. Procedia* **2012**, *26*, 284–293. [CrossRef]
8. Lesea, A.; Drimer, S.; Fabula, J.J.; Carmichael, C.; Alfke, P. The Rosetta experiment: Atmospheric soft error rate testing in differing technology FPGAs. *IEEE Trans. Dev. Mat. Reliab.* **2005**, *5*, 317–328. [CrossRef]
9. Lesea, A.; Castellani-Coulié, K.; Waysand, G.; Le Mauff, J.; Sudre, C. Qualification Methodology for Sub-Micron ICs at the Low Noise Underground Laboratory of Rustrel. *IEEE Trans. Nucl. Sci.* **2008**, *55*, 2148–2153. [CrossRef]
10. Xilinx. Continuing Experiments of Atmospheric Neutron Effects on Deep Submicron Integrated Circuits WP286 (v1.1). 13 October 2011. Available online: https://citeseerx.ist.psu.edu/document?repid=rep1&type=pdf&doi=51222cecfc39e38d06cf94d6f95c462ecf910a2d (accessed on 3 March 2023).
11. Chen, W.; Guo, X.; Wang, C.; Zhang, F.; Qi, C.; Wang, X.; Jin, X.; Wei, Y.; Yang, S.; Song, Z. Single-event upsets in SRAMs with scaling technology nodes induced by terrestrial, nuclear reactor, and monoenergetic neutrons. *IEEE Trans. Nucl. Sci.* **2019**, *66*, 856–865. [CrossRef]
12. Chen, W. Irradiation testing and simulation of neutron-induced single event effects. In Proceedings of the 26th International Seminar on Interaction of Neutrons with Nuclei, Xi'an, China, 28 May–1 June 2018.
13. Zhang, J.L.; Tan, Y.H.; Wang, H.; Lu, H.; Meng, X.C.; Muraki, Y. The Yangbajing muon–neutron telescope. *Nucl. Inst. Meth. Phys. Res. A* **2010**, *623*, 1030–1034. [CrossRef]

14. Jin, X.M.; Chen, W.; Li, J.L.; Qi, C.; Guo, X.Q.; Li, R.B.; Liu, Y. Single event upset on static random access memory devices due to spallation, reactor, and monoenergetic neutrons. *Chin. Phys. B* **2019**, *28*, 104212. [CrossRef]
15. Andreani, C.; Senesi, R.; Paccagnella, A.; Bagatin, M.; Gerardin, S.; Cazzaniga, C.; Frost, C.D.; Picozza, P.; Gorini, G.; Mancini, R.; et al. Fast neutron irradiation tests of flash memories used in space environment at the ISIS spallation neutron source. *AIP Adv.* **2018**, *8*, 025013. [CrossRef]
16. Hu, Z.L.; Yang, W.T.; Zhou, B.; Liu, Y.N.; He, C.; Wang, S.L.; Yu, Q.Z.; Liang, T.J. Neutron-induced single event effect in Xilinx 16nm MPSoC configuration RAM (CRAM) using white neutron and 2.72~81.8meV neutron in CSNS-BL20. *J. Nucl. Sci. Technol.* **2023**, *60*, 473–478. [CrossRef]
17. Baumann, R.C.; Smith, E.B. Neutron-induced ^{10}B fission as a major source of soft errors in high density SRAMs. *Microelectron. Reliab.* **2001**, *41*, 211. [CrossRef]
18. Lucas, M.L.; Daniel, S.; Helmut, P.; Rubén, G.A.; Manon, L.; Carlo, C.; Alberto, B.; Luigi, D. Neutron-induced effects on a self-refresh DRAM. *Microelectron. Reliab.* **2022**, *128*, 114406.
19. Kumar, S.; Agarwal, S.; Jung, J.P. Soft error issue and importance of low alpha solders for microelectronics packaging. *Rev. Adv. Mater. Sci.* **2013**, *34*, 185–202.
20. Wen, S.J.; Pai, S.Y.; Wong, R.; Romain, M.; Tam, N. B10 finding and correlation to thermal neutron soft error rate sensitivity for SRAMs in the sub-micron technology. In Proceedings of the IEEE International Integrated Reliability Workshop Final Report, South Lake Tahoe, CA, USA, 15–18 October 2010.
21. Cecchetto, M.; Alía, R.G.; Wrobel, F.; Tali, M.; Stein, O.; Lerner, G.; Bilko, K.; Esposito, L.; Castro, C.B.; Kadi, Y.; et al. Thermal neutron-induced SEUs in the LHC accelerator environment. *IEEE Trans. Nucl. Sci.* **2020**, *67*, 1412–1420. [CrossRef]
22. Weulersse, C.; Houssany, S.; Guibbaud, N.; Segura-Ruiz, J.; Beaucour, J.; Miller, F.; Mazurek, M. Contribution of Thermal Neutrons to Soft Error Rate. *IEEE Trans. Nucl. Sci.* **2018**, *65*, 1851–1857. [CrossRef]
23. Fang, Y.P.; Oates, A.S. Thermal neutron-induced soft errors in advanced memory and logic devices. *IEEE Trans. Device Mater. Rel.* **2014**, *14*, 583–586. [CrossRef]
24. Yamazaki, T.; Kato, T.; Uemura, T.; Matsuyama, H.; Tada, Y.; Yamazaki, K.; Soeda, T.; Miyajima, T.; Kataoka, Y. Origin analysis of thermal neutron soft error rate at nanometer scale. *J. Vac. Sci. Technol. B* **2015**, *33*, 020604. [CrossRef]
25. Hu, Z.; Yang, W.; Li, Y.; Li, Y.; He, C.; Wang, S.; Zhou, B.; Yu, Q.; He, H.; Xie, F.; et al. Atmospheric neutron single event effect in 65 nm microcontroller units by using CSNS-BL09. *Acta Phys. Sin.* **2019**, *68*, 238502. [CrossRef]
26. Brookhaven National Laboratory; National Nuclear Data Center (NNDC); Evaluated Nuclear Data File (ENDF). Available online: https://www.nndc.bnl.gov/endf/ (accessed on 2 February 2023).
27. Yang, W.; Li, Y.; Li, Y.; Hu, Z.; Xie, F.; He, C.; Wang, S.; Zhou, B.; He, H.; Khan, W.; et al. Atmospheric Neutron Single Event Effect Test on Xilinx 28nm System on Chip at CSNS-BL09. *Microelectron. Reliab.* **2019**, *99*, 119–124. [CrossRef]
28. Chen, Y. China Spallation Neutron Source. *Bull. Chin. Acad. Sci.* **2011**, *26*, 726–729.
29. Yu, Q.; Shen, F.; Yuan, L.; Lin, L.; Hu, Z.; Zhou, B.; Liang, T. Physical design of an Atmospheric Neutron Irradiation Spectrometer at China Spallation Neutron Source. *Nucl. Eng. Des.* **2022**, *386*, 111579. [CrossRef]
30. Orban, J.; Fuzi, J.; Rosta, L. Development of area detectors for neutron beam instrumentation at the Budapest neutron centor, 2020, IAEA-TECDOC-1935, Modern Neutron Detection Proceedings of a Technical Meeting, Vienna, Austria. Available online: https://www-pub.iaea.org/MTCD/Publications/PDF/TE-1935_web.pdf (accessed on 1 February 2023).
31. Hunt, S.; Iliadis, C.; Longland, R. Characterization of a 10B-doped liquid scintillator as a capture-gated neutron spectrometer. *Nucl. Instrum. Methods Phys. Res. Sect. A Accelerators. Spectrometers Detect. Assoc. Equip.* **2016**, *811*, 108–114. [CrossRef]
32. SRIM. Particle Interactions with Matter. 2013. Available online: http://www.srim.org/ (accessed on 4 March 2023).
33. Yang, W.; Yin, Q.; Li, Y.; Guo, G.; Li, Y.H.; He, C.H.; Zhang, Y.W.; Zhang, F.Q.; Han, J.H. Single-event effects induced by medium-energy protons in 28 nm system-on-chip. *Nucl. Sci. Technol.* **2019**, *30*, 151. [CrossRef]
34. Amrbar, M.; Irom, F.; Guertin, S.M.; Allen, G. Heavy ion single event effects measurements of Xilinx Zynq-7000 FPGA. In Proceedings of the IEEE Radiation Effects Data Workshop (REDW), Boston, MA, USA, 13–17 July 2015.
35. Di Mascioa, S.; Menicuccia, A.; Furano, G.; Szewczyk, T.; Campajola, L.; Di Capua, F.; Lucaroni, A.; Ottavi, M. Towards defining a simplified procedure for COTS system-on-chip TID testing. *Nucl. Eng. Technol.* **2018**, *50*, 1298–1305. [CrossRef]
36. Leroy, C.; Rancoita, P.G. *Principles of Radiation Interaction in Matter and Detection*, 2nd ed.; Word Scientific Publishing: Singapore, 2009.
37. Uwe, S.; Hwang, C.S.; Funakubo, H. *Ferroelectricity in Doped Hafnium Oxide: Materials, Properties and Devices*; Woodhead Publishing: Sawston, UK, 2019.
38. Czernohorsky, M.; Seidel, K.; Kühnel, K.; Niess, J.; Sacher, N.; Kegel, W.; Lerch, W. High-K metal gate stacks with ultra-thin interfacial layers formed by low temperature microwave-based plasma oxidation. *Microelectron. Eng.* **2017**, *178*, 262–265. [CrossRef]
39. Agostinelli, S.; Allison, J.; Amako, K.; Apostolakis, J.; Araujo, H.; Arce, P.; Asai, M.; Axen, D.; Banerjee, S.; Barrand, G.; et al. GEANT4-a simulation toolkit. *Nucl. Instrum. Methods Phys. Res. A* **2003**, *506*, 250–303. [CrossRef]
40. Yang, W.; Li, Y.; Zhang, W.; Guo, Y.; Zhao, H.; Wei, J.; Li, Y.; He, C.; Chen, K.; Guo, G. Electron inducing soft errors in 28 nm system-on-Chip. *Radiat. Eff. Defects Solids* **2020**, *175*, 745–754. [CrossRef]